Journal of Materials Chemistry C

Accepted Manuscript

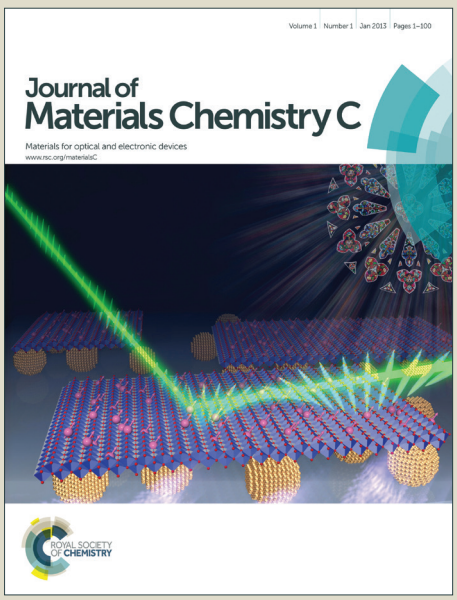

ROYAL SOCIETY OF CHEMISTRY

www.rsc.org/materialsC

Journal Name

RSCPublishing

ARTICLE

Design and Optical Investigations of a Spironaphthoxazine/Polyoxometalate/Spiropyran Triad

Cite this: DOI: 10.1039/xoxxoooooox

Received ooth January 2012,
Accepted ooth January 2012

DOI: 10.1039/xoxxoooooox

www.rsc.org/

Ali Saad,[a] Olivier Oms,*[a] Jérôme Marrot,[a] Anne Dolbecq,[a] Khadija Hakouk,[b] Houda El Bekkachi,[b] Stéphane Jobic,[b] Philippe Deniard,[b] Rémi Dessapt,*[b] Damien Garrot,[c] Kamel Boukheddaden,[c] Rongji Liu,[d] Guangjin Zhang,*[d] Bineta Keita[e] and Pierre Mialane[a]

The assembly of two distinct organic photochromic groups and a polyoxometalate (POM) within a single molecule has been realized. In the hetero-functionalized Anderson polyanion **$MnMo_6O_{18}(SP)(SN)$**, one spiropyran and one spironaphthoxazine cap the two faces of a planar $\{Mn^{III}Mo_6{}^{VI}O_{18}\}$ fragment. A related symmetrical POM where the $\{Mn^{III}Mo_6{}^{VI}O_{18}\}$ inorganic moiety is connected to two spironaphthoxazines has also been obtained, and isolated as an organoammonium (**$MnMo_6O_{18}(SN)_2$**) or a cationic spiropyran (**$(SP)_3MnMo_6O_{18}(SN)_2$**) salt. The structures of **$MnMo_6O_{18}(SN)_2$** and **$MnMo_6O_{18}(SP)(SN)$** have been solved by single-crystal X-ray diffraction analysis. In solution, both compounds exhibit electrochromic properties with multiple redox coloured states. The solid-state photochromism of all the compounds has also been extensively studied at room temperature. Contrary to the organic spironaphtoxazine derivative **SNTris** which is very poorly photochromic, the pale yellow colour of **$MnMo_6O_{18}(SN)_2$** shifts to deep blue with high coloration contrast which underlines the positive effect of the grafting onto the inorganic platform. In addition, **$MnMo_6O_{18}(SN)_2$** shows also a good cyclability and exhibits a fast bleaching process. Finally, the temperature dependence of the solid-state photochromic properties of **$MnMo_6O_{18}(SN)_2$** is also reported and compared to that of the related **$MnMo_6O_{18}(SP)_2$**. The photo-coloration process which is attenuated at low temperature in both cases is clearly more affected for **$MnMo_6O_{18}(SN)_2$**. Moreover, the thermal fading process becomes significant at 340 K for **$MnMo_6O_{18}(SP)_2$** and 260 K for **$MnMo_6O_{18}(SN)_2$** underlining strong different optical behaviours between both materials.

1. Introduction

Polyoxometalates (POMs) are generally described as soluble metal oxides of early transition metals (usually W, Mo, V) in high oxidation states.[1] The huge diversity of their compositions and structures make them relevant for applications in numerous fields, which include catalysis,[2] biological activity,[3] magnetism[4] and materials science.[5] They have also been widely studied for their rich optical properties.[6] In particular, it is known since decades that when associated with organoammonium cations, polyanions may exhibit highly tunable photochromic properties in the crystalline state, with strong colour changes. In addition, we have shown recently that effective solid-state photochromic materials can also be obtained by combining POMs and sulfonium cations.[7] In all these systems, the color change is due to photoreduction of Mo^{6+} ions which arises from an UV-induced electron transfer inside the POM moiety, the organic counterion acting as a stabilizer of the reduced POM. In contrast, we have recently developed a family of compounds where both the organic and inorganic parts participate to the coloration of the irradiated material. We first characterized a series of hybrid materials in which polyanions are ionically associated to cationic spiropyrans, a well-known class of photochromic organic compounds.[8] Under UV irradiation, the weak C_{spiro}-O bond characterizing these molecules is easily broken, and the non-planar closed "spiro" form (SP), which is usually uncoloured, is converted into the highly coloured planar opened "merocyanine" form (MC). Noticeably, polyanions, as well as spiropyrans, can also exhibit electrochromic properties. Indeed, the association of $[PM_{12}O_{40}]^{3-}$ (M = W, Mo) Keggin polyanions

and spiropyran cations has led to ionic hybrid materials exhibiting dual photochromic and electrochromic properties, both in solution and in the crystalline state. However, in the solid state, the slowness of the photoresponse of the POM moiety has been evidenced.[9a] Nevertheless, using the same spiropyran cation but the intrinsically photochromic bisphosphonato polyoxomolybdate $[(Mo_3O_8)_4(O_3PC(C_3H_6NH_3)(O)PO_3)_4]^{8-}$ instead of Keggin units, a ionic compound exhibiting improved photochromic performances has been obtained.[9b] We have then evidenced strong synergetic effects between the optical properties of both the POM and the SP moieties.[9c] Noticeably, the efficiency of the SP ⇆ MC photoisomerization can be finely tuned playing with the nature of the POM units and the design of the supramolecular hybrid frameworks. Finally, in order to gather in a single molecule the optical properties of POMs and spiropyrans, compounds where the two components are covalently connected have been developed.[10]

In particular, the multichromic hybrid compounds $(TBA)_3[MnMo_6O_{18}\{(OCH_2)_3CNH_2\}\{(OCH_2)_3CNHC_{21}H_{19}N_2O_4\}]$ (**$MnMo_6O_{18}(SP)$**) and $(TBA)_3[MnMo_6O_{18}\{(OCH_2)_3CNHC_{21}H_{19}N_2O_4\}_2]$ (**$MnMo_6O_{18}(SP)_2$**) have been successfully synthesized (TBA = tetrabutylammonium cation).[10a] These molecular systems were obtained by covalently grafting – via peptide coupling – a spiropyran carboxylic acid derivative onto the $\{MnMo_6O_{18}\}$ Anderson-type polyoxomolybdate platform which possesses two free amino groups.

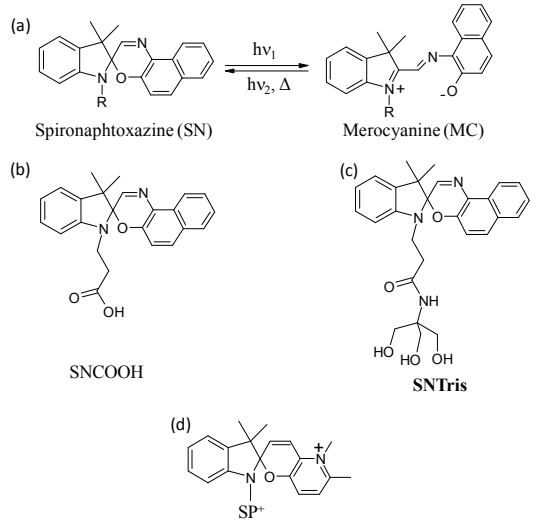

Fig. 1 a) Photoinduced equilibrium involving a spironaphthoxazine derivative; representations of b) SNCOOH; c) **SNTris**; d) the cationic spiropyran acting as counter-ion in **$(SP)_3MnMo_6O_{18}(SN)_2$** and in **(SP)I**.

Under low-power UV excitation, **$MnMo_6O_{18}(SP)$** and **$MnMo_6O_{18}(SP)_2$** develop a strong solid-state photochromic effect at room temperature with a remarkable coloration contrast and a fast coloration speed, and they are quite bistable photoactive molecular switches. Besides, spectroelectrochemical measurements highlighted the existence of six different stable redox states for **$MnMo_6O_{18}(SP)$**. But overall, this compound possesses a free amino group, opening the way for a further functionalization of this species, and thus offering a unique opportunity to elaborate a hybrid system incorporating three different optically active groups in a single molecule.

Herein we report the grafting of a spironaphthoxazine (SN) molecule onto the **$MnMo_6O_{18}(SP)$** platform. As for spiropyran compounds, spironaphthoxazines exhibit high fatigue resistance,[11] and materials based on such species have been considered for diverse potential applications, such as optical data storage,[12] sensors[13] and switches.[14] Also, this class of compounds is characterized by a photochromic mechanism closely related to that of spiropyrans. Indeed, under UV light, a cleavage of the C_{spiro}-O bond and the generation of a coloured merocyanine form exhibiting extended conjugation through the central azomethine bridge are observed (Fig. 1a). However, the spiropyran and spironaphthoxazine species chosen here exhibit clearly distinct optical properties. The synthesis and the structural characterization of the unsymmetrical hybrid POM triad $(TBA)_3[MnMo_6O_{18}\{(OCH_2)_3CNHC_{21}H_{19}N_2O_4\}\{(OCH_2)_3CNHC_{24}H_{21}N_2O_2\}]$ (**$MnMo_6O_{18}(SP)(SN)$**) are thus reported. The related symmetrical hybrid complex $(TBA)_3[MnMo_6O_{18}\{(OCH_2)_3CNHC_{24}H_{21}N_2O_2\}_2]$ (**$MnMo_6O_{18}(SN)_2$**), which contains two spironaphthoxazines groups, has also been characterized. In addition, the ionic compound $(C_{20}H_{23}N_2O)_3[MnMo_6O_{18}\{(OCH_2)_3CNHC_{24}H_{21}N_2O_2\}_2]$ (**$(SP)_3MnMo_6O_{18}(SN)_2$**) has been obtained from **$MnMo_6O_{18}(SN)_2$**, by substituting the TBA counter-ions by spiropyran cations. The optical properties of all these compounds are widely discussed and compared.

2. Results and discussion

2.1 Synthesis and structural description

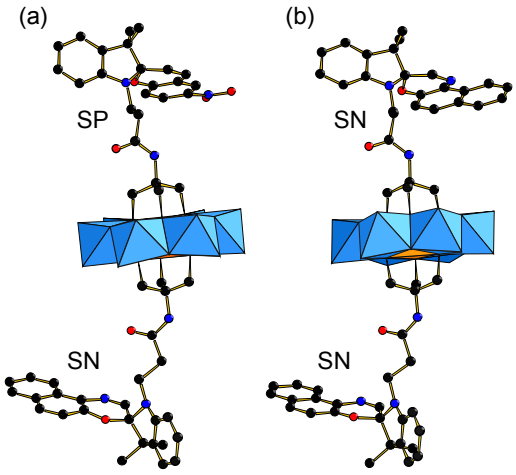

Fig. 2 Mixed polyhedral and ball-and-stick representations of the anionic unit in: (a) **$MnMo_6O_{18}(SP)(SN)$**, (b) **$MnMo_6O_{18}(SN)_2$**. Blue octahedra, $\{MoO_6\}$; orange octahedron, $\{MnO_6\}$; red spheres, O; blue spheres, N; black spheres, C. H atoms have been omitted for clarity.

Among the few routes leading to covalently linked hybrid POMs,[15] the functionalization of Anderson-type polyoxomolybdates has been probably the most extensively considered.[16] Recently, we have described the **$MnMo_6O_{18}$(SP)** polyoxometalate, which possesses a free amino group.[10a] The reaction of this complex with the spironaphthoxazine carboxylic acid derivative SNCOOH[17] (Fig. 1b) via a peptide coupling reaction affords the **$MnMo_6O_{18}$(SP)(SN)** compound. Single crystals were obtained by slow diffusion of diethylether into an acetonitrile solution of **$MnMo_6O_{18}$(SP)(SN)**.

An X-ray diffraction analysis (Table SI1 in the Supporting Information) confirmed that one SN entity has been grafted onto the inorganic platform *via* the formation of an amide function, the SP group remaining on the other side of the $\{MnMo_6O_{18}\}$ core (Fig. 2a). **$MnMo_6O_{18}$(SP)(SN)** thus represents a rare example of hetero-functionalized Anderson POM derivative.[16e,g,n] As expected, the C_{spiro}-O bonds (1.543(5) Å for the SP group and 1.470(6) Å for the SN entity) are longer than usual C_{sp^3}-O bonds.

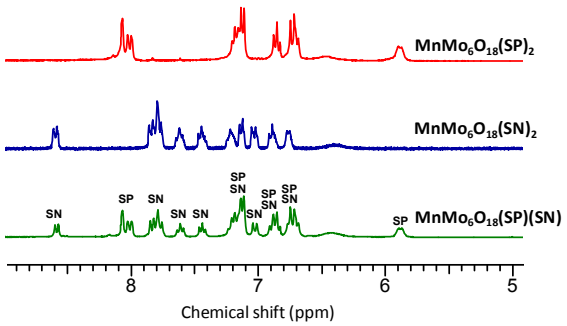

Fig. 3 Compared ^{1}H NMR (CD_3CN) spectra of **$MnMo_6O_{18}$(SP)$_2$**, **$MnMo_6O_{18}$(SN)$_2$** and **$MnMo_6O_{18}$(SP)(SN)** (5-9 ppm range).

A solution ^{1}H NMR spectrum of **$MnMo_6O_{18}$(SP)(SN)** clearly indicates a SN:SP ratio of 1:1 (Fig. 3, the whole ^{1}H NMR spectrum is shown in Fig. SI1 in the Supporting Information). Especially, the sets of the signals for the aromatic protons of the two organic fragments can be easily distinguished by comparison with the spectra of the pure spiropyran derivative **$MnMo_6O_{18}$(SP)$_2$** previously reported[10a] and of the pure spironaphthoxazine compound **$MnMo_6O_{18}$(SN)$_2$** reported here (see below). The solution ^{13}C NMR spectrum of **$MnMo_6O_{18}$(SP)(SN)** (Fig. SI2 in the Supporting Information) is also in agreement with the solid-state structure of this complex, exhibiting in particular two peaks at 172.2 ppm and 171.8 ppm for the two carbon atoms of the carbonyl groups, while only one peak is observed for the symmetrical hybrid Anderson-type POMs **$MnMo_6O_{18}$(SN)$_2$** (see below) and **$MnMo_6O_{18}$(SP)$_2$**. Both these NMR experiments thus assess the purity of the reported material as well as its stability in solution.

In order to accurately interpret the photochromic properties of **$MnMo_6O_{18}$(SP)(SN)**, the pure spironaphthoxazine derivative **$MnMo_6O_{18}$(SN)$_2$** in which each face of the $\{MnMo_6O_{18}\}$ fragment is capped by a SN group, has also been prepared. The synthesis procedure consists in a peptide coupling reaction between the $(TBA)_3[MnMo_6O_{18}\{(OCH_2)_3CNH_2\}_2]$ precursor[16b] and an excess of SNCOOH. Crystals of **$MnMo_6O_{18}$(SN)$_2$** have been isolated following the same recrystallization protocol than that used for **$MnMo_6O_{18}$(SP)(SN)**, and this compound has been crystallographically characterized (Table SI2 in the Supporting Information).

Interestingly, the functionalized $\{MnMo_6O_{18}\}$ units exhibit a very similar structural arrangement in **$MnMo_6O_{18}$(SP)(SN)** and **$MnMo_6O_{18}$(SN)$_2$**. As observed for **$MnMo_6O_{18}$(SP)(SN)**, the spironaphthoxazine entities grafted onto the $\{MnMo_6O_{18}\}$ platform in **$MnMo_6O_{18}$(SN)$_2$** possess quite long C_{spiro}-O bonds (1.536(10) and 1.45(8) Å) (Fig. 2b). As expected, the solution ^{13}C NMR spectrum of this symmetrical hybrid shows a single peak relative to the amide functions at 171.7 ppm (Fig. SI2 in the Supporting Information). In addition to these hybrid systems, in order to study the effect of the polyoxomolybdate part on the photochromic properties of the SN fragment in **$MnMo_6O_{18}$(SP)(SN)** and **$MnMo_6O_{18}$(SN)$_2$**, the purely organic spironaphthoxazine compound **SNTris** (Fig. 1c) has also been prepared, by reacting SNCOOH with tris (tris = 2-amino-2-(hydroxymethyl)-1,3-propanediol). In this species, the amide function linked to the photochromic part mimics the chemical environment of the spironaphthoxazine in the related POM materials, allowing potentially discriminating the different roles on the optical properties of the fragments constituting these compounds.

$(SP)_3MnMo_6O_{18}$(SN)$_2$ has been synthesized by substituting by cationic spiropyrans (Fig. 1d) the TBA cations of **$MnMo_6O_{18}$(SN)$_2$**. This compound has been obtained in good yield and without any trace of starting material by addition of a large excess (20 eq.) of spiropyran cations. It has not been possible to obtain single-crystals of **$(SP)_3MnMo_6O_{18}$(SN)$_2$** suitable for single-crystal X-ray diffraction analysis. However, solution NMR experiments allowed assessing the formulation of this species. First, the ^{1}H NMR spectrum of **$(SP)_3MnMo_6O_{18}$(SN)$_2$** (Fig. SI3 in the Supporting Information) shows no signal relative to TBA cations. In addition, the SN:SP (2:3) ratio evaluated from the relevant signals of the two entities matches very well with the expected formulae anticipated from charge considerations. Secondly, the ^{13}C NMR spectrum (Fig. SI4 in the Supporting Information) confirms the absence of TBA cations in the final product, and the integrity of the $[MnMo_6O_{18}(SN)_2]^{3-}$ anion. In contrast with **$MnMo_6O_{18}$(SP)(SN)**, **$(SP)_3MnMo_6O_{18}$(SN)$_2$** thus represents a material where spiropyran molecules are ionically interacting with a spironaphthoxazine/POM entity. Finally, elemental analysis corroborates the purity of all the compounds reported here.

2.2 Electrochemical and spectroelectrochemical characterization

Cyclic voltammetry (CV), controlled potential coulometry, and UV-vis NIR spectrometry were used for electrochemical and spectroelectrochemical characterization of **$MnMo_6O_{18}$(SN)$_2$**,

$MnMo_6O_{18}(SP)(SN)$ and **SNTris** in DMF in the presence of $LiClO_4$.

All the compounds have electro-oxidizable (Mn, SN and SP) or electro-reducible (Mn, SN, SP and Mo) centers. For clarity, these redox processes are described separately.

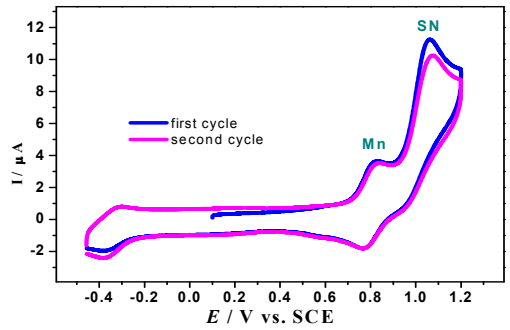

Fig. 4 Oxidation cyclic voltammograms (first two cycles) of 0.3 mM **$MnMo_6O_{18}(SN)_2$** (Mn and SN centers). The electrolyte was DMF + 0.2M $LiClO_4$.The reference electrode was a saturated calomel electrode (SCE). The scan rate was 0.1V s^{-1}.

In the positive potential domain (versus SCE) the CV pattern of **$MnMo_6O_{18}(SN)_2$** is composed of two well-defined waves peaking respectively at +0.830 V and +1.060 V versus SCE and relevant to the oxidation of the Mn^{III} and SN respectively (Fig. 4). It is worth noting that the Mn^{IV}/ Mn^{III} redox process is quasi-reversible (the anodic-to-cathodic peak potential difference at 0.1Vs^{-1} ΔEp = 0.080 V) and its peak current intensities vary linearly with the square root of the scan rate as expected for electron transfer governed by diffusion process. Fig. 4 also exhibits a quasi-reversible wave located at -0.380 V versus SCE which is attributed to a new compound produced along with the oxidation of the SN centers. Indeed, Fig. SI5 (in the Supporting Information) shows that such redox couple is not observed upon restriction of the potential domain to the Mn^{III} to Mn^{IV} process. The decrease of the SN peak intensity during the second scan of the CV underscores the transformation accompanying its oxidation (Fig. 4). Similar behaviours were also observed for **$MnMo_6O_{18}(SP)(SN)$**, however, its CV patterns display different features which allow to clearly distinguish them. As a main difference, Fig. SI6 (in the Supporting Information) indicates that the oxidation of the SP and SN centers within **$MnMo_6O_{18}(SP)(SN)$** proceeds through two steps featured by two closely spaced waves. These processes are assigned respectively to the oxidation waves of the SN (ca.+1.035 V versus SCE) and SP (+1.095 V versus SCE) centers. Furthermore the overall electron transfer process estimated from the anodic-to-cathodic peak potential differences of the Mn^{IV}/Mn^{III} redox couple is slightly faster for **$MnMo_6O_{18}(SN)_2$** (ΔEp = 0.080 V) than for **$MnMo_6O_{18}(SP)(SN)$** (ΔEp = 0.100 V). The reduction waves of **$MnMo_6O_{18}(SN)_2$**, **$MnMo_6O_{18}(SP)(SN)$** and **SNTris** located before the electrolyte discharge are presented on Fig. SI7A, SI7B and SI8 (in the Supporting Information) respectively. The CV of **SNTris** presents a single reduction wave at -1.860 V versus SCE while that of **$MnMo_6O_{18}(SN)_2$** exhibits three well-defined reduction waves peaking at -1.000 V, -1.700 V and -2.010 V versus SCE respectively. These waves are attributed to the reduction of the Mn, SN and Mo centers respectively. In contrast, the CV pattern of **$MnMo_6O_{18}(SP)(SN)$** displays a broad composite reduction wave featuring the partial merging of the reduction processes of the Mn, SP and SN centers. This observation is in accordance with the behaviour reported for **$MnMo_6O_{18}(SP)_2$**.[10a]

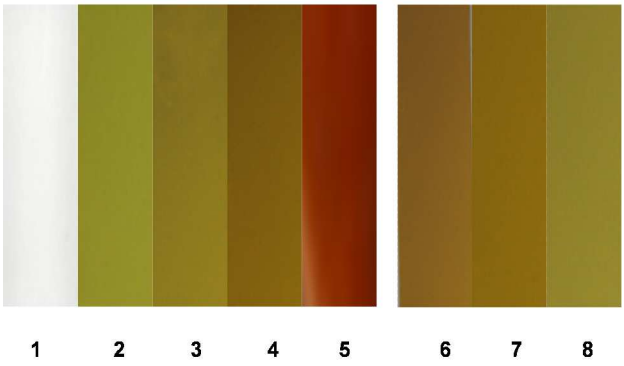

Fig. 5 Observed color nuances for 0.15 mM **$MnMo_6O_{18}(SN)_2$**: (1) before electrolysis; (2 - 5) coloration during electro-oxidation; (6 - 8) electrochemical fading process by reduction.

The electronic absorption spectra of the three compounds are represented on Fig. SI9 (in the Supporting Information). The main absorption spectra characteristics of these species are given in Table SI3 (in the Supporting Information). In particular, it is observed that for **$MnMo_6O_{18}(SP)(SN)$** the SN peak at 372 nm is merged with that of SP.

Fig. 5 features the multiple colored states observed during the electro-oxidation of **$MnMo_6O_{18}(SN)_2$** at + 1.2 V versus SCE. Electroreduction of the resulting solution could not restore the greyish-white color of **$MnMo_6O_{18}(SN)_2$** even at a highly negative potential (-1.2 V versus SCE). This result is in agreement with that observed by CV which indicates that **$MnMo_6O_{18}(SN)_2$** undergoes a transformation upon successive potential cycling in the potential domain related to its SN centers. The yellowish-green color might be due to the new compound obtained during this process. It is worth noting that this color is stable during several hours. Moreover, the multiple colored states could be repeatedly observed. The complex **$MnMo_6O_{18}(SP)(SN)$** exhibits similar properties, however, its color sets, as represented in Fig. SI10 (in the Supporting Information), are slightly different compared to that of **$MnMo_6O_{18}(SN)_2$**. This observation is attributed to the presence of SN and SP groups within **$MnMo_6O_{18}(SP)(SN)$**. As expected, the color sets observed for the SN group within **SNTris**, are also different to those of these two complexes (Fig. SI11 in the Supporting Information). The spectra of the oxidised forms of the three compounds display a peak at 460 nm followed by a shoulder at ca. 600 nm. However, as the structures of these oxidised forms are unknown, the studies of the mechanistic

pathways of the formation of the compounds which induce the color sets are beyond the scope of the present work.

2.3 Room temperature solid-state photochromic properties

The solid-state photochromic properties of **$MnMo_6O_{18}(SP)(SN)$**, **$MnMo_6O_{18}(SN)_2$**, **$(SP)_3MnMo_6O_{18}(SN)_2$** and the organic references **SNTris** and the iodide salt of the spiropyran cation, **(SP)I** represented on Fig. 1d, have been investigated in ambient conditions by diffuse reflectance spectroscopy of microcrystalline powders. Before UV irradiation, the absorption spectra of **$MnMo_6O_{18}(SN)_2$** is the perfect superimposition of those of the nonphotochromic precursor $(TBA)_3[MnMo_6O_{18}\{(OCH_2)_3CNH_2\}_2]$ and **SNTris** (Fig. SI12a in the Supporting Information). The optical gap of **$MnMo_6O_{18}(SN)_2$** arises at 396 nm and is mainly attributable to the absorption of the SN moiety. By comparison, **$(SP)_3MnMo_6O_{18}(SN)_2$** shows a similar optical gap (398 nm) but this is strongly dominated by the intense absorption of the SP^+ counter-cations, as already observed in $SP_7Na[(Mo_3O_8)_4(O_3PC(C_3H_6NH_3)(O)PO_3)_4]\cdot 30H_2O$[9b] (Fig. SI12b in the Supporting Information) and in other SP/POM supramolecular assemblies.[9c] In contrast, the optical gap of **$MnMo_6O_{18}(SP)(SN)$** is located at lower energy (424 nm), similarly as observed for **$MnMo_6O_{18}(SP)_2$**,[10a] which reveals that the SP moiety dictates the absorption threshold in **$MnMo_6O_{18}(SP)(SN)$** (Fig. SI13 in the Supporting Information).

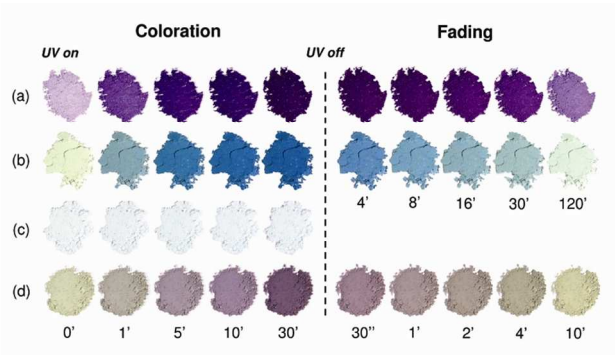

Fig. 6 Photographs of powders of (a) **$MnMo_6O_{18}(SP)(SN)$**, (b) **$MnMo_6O_{18}(SN)_2$**, (c) **SNTris**, and (d) **$(SP)_3MnMo_6O_{18}(SN)_2$** at different time (in min) during the coloration process under 365-nm UV irradiation (left), and the fading process under ambient light at room temperature (right). Let us notice that before UV irradiation, the pinkish color of **$MnMo_6O_{18}(SP)(SN)$** is assignable to a small amount of the opened "merocyanine" form of the SP group.

As shown in Fig. 6, **$MnMo_6O_{18}(SP)(SN)$**, **$MnMo_6O_{18}(SN)_2$**, and **$(SP)_3MnMo_6O_{18}(SN)_2$** show strong solid-state photochromic effects at room temperature. Under low-power UV irradiation (365 nm, 6 W) the grayish-white powder of **$MnMo_6O_{18}(SN)_2$** quickly shifts to deep blue while in marked contrast, the color change of the pure organic **SNTris** is quasi undetectable by human eyes, even after irradiating the sample for a period as long as few hours. This clearly evidences that highly effective solid-state photochromic hybrid materials can be reached by grafting onto the $\{MnMo_6O_{18}\}$ platform spiro-derivatives initially very weakly photochromic in the crystalline state.

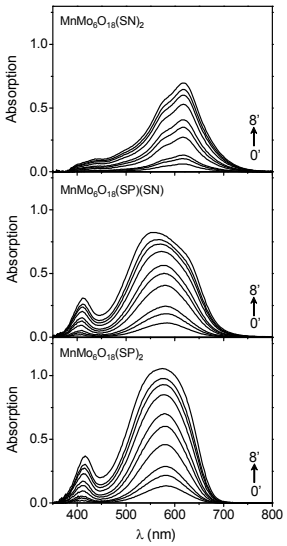

Fig. 7 Temporal evolution of the photogenerated absorption of **$MnMo_6O_{18}(SN)_2$**, **$MnMo_6O_{18}(SP)(SN)$**, and **$MnMo_6O_{18}(SP)_2$** after 0, 0.166, 0.333, 0.5, 1, 1.5, 2, 3, 4, 5, and 8 min of 365 nm-UV irradiation.

Under similar UV exposure, the powders of **$(SP)_3MnMo_6O_{18}(SN)_2$** and **$MnMo_6O_{18}(SP)(SN)$** quickly develop a deep red-purple and a deep bluish-purple color, respectively. Let us notice that this latter differs from the red-purple color of **$MnMo_6O_{18}(SP)_2$** once irradiated (see below).[10a] After switching off the UV excitation, the bleaching processes occur under ambient light and at room temperature, with different rates. Noticeably, the UV-induced coloration of **$(SP)_3MnMo_6O_{18}(SN)_2$** totally fades in ten minutes, revealing a very fast reversible system. The blue color of **$MnMo_6O_{18}(SN)_2$** gradually fades to fully disappear in about 150 min, while the bleaching of **$MnMo_6O_{18}(SP)(SN)$** arises more slowly.

To better characterize the color-change effect, Fig. 7 displays the evolution of the photogenerated absorption with the UV irradiation time for **$MnMo_6O_{18}(SN)_2$**, **$MnMo_6O_{18}(SP)(SN)$**, and **$MnMo_6O_{18}(SP)_2$** used as a reference in this work. An absorption band grows up at λ_{max} = 620 nm for **$MnMo_6O_{18}(SN)_2$**, which is characteristic of the MC form of the SN group, similarly as observed for **SNTris** (Fig. SI14 in the Supporting Information). By comparison, the MC form of the SP moiety in **$MnMo_6O_{18}(SP)_2$** is characterized by two bands, the first small one at λ_{max} = 410 nm, and a second much more intense one at λ_{max} = 570 nm. The photogenerated absorption of **$MnMo_6O_{18}(SN)_2$** is less intense than that at λ_{max} = 570 nm for **$MnMo_6O_{18}(SP)_2$**, showing a less pronounced photochromic effect for the spironaphthoxazine-derivative, even if the coloration contrast in **$MnMo_6O_{18}(SN)_2$** nevertheless remains noticeable.

Very interestingly, the absorption spectra of **$MnMo_6O_{18}(SP)(SN)$** clearly show three bands at λ_{max} = 410 nm, 570 nm (the dominant one), and 620 nm, revealing that both the SN and SP moieties are photoactive.

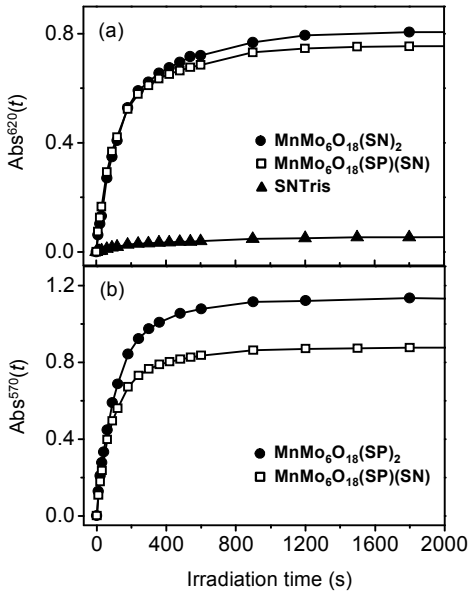

Fig. 8 (a) $Abs^{620}(t)$ vs. t plots for $\mathbf{MnMo_6O_{18}(SN)_2}$, $\mathbf{MnMo_6O_{18}(SP)(SN)}$, and **SNTris**. (b) $Abs^{570}(t)$ vs. t plots for $\mathbf{MnMo_6O_{18}(SP)(SN)}$, and $\mathbf{MnMo_6O_{18}(SP)_2}$. The lines show the fits of the plots according to rate law $Abs^{\lambda max}(t) = -(A_1 + A_2) + A_1exp(-k^c_1t) + A_2exp(-k^c_2t)$.

Due to the superimposition of the bands at λ_{max} = 570 nm and 620 nm, the absorption in the range 450-700 nm is broader than that of $\mathbf{MnMo_6O_{18}(SP)_2}$, which explains the difference in color of the two compounds. $\mathbf{(SP)_3MnMo_6O_{18}(SN)_2}$ develops a broad absorption at λ_{max} = 584 nm which is comparable with that of the **(SP)I** precursor once irradiated (Fig. SI15 in the Supporting Information). The band at λ_{max} = 620 nm is not distinguishable for $\mathbf{(SP)_3MnMo_6O_{18}(SN)_2}$ quite showing that its photoresponse is mainly dominated by the absorption of the MC form related to the SP^+ counter-cations.

The photocoloration kinetics of the spironaphthoxazine and spiropyran groups in the hybrid materials have been quantified at room temperature from the evolution of the absorption at λ_{max} = 620 nm ($Abs^{620}(t)$) for the SN group, λ_{max} = 570 nm ($Abs^{570}(t)$) for the SP group, and λ_{max} = 584 nm ($Abs^{584}(t)$) for the SP^+ counterion, as a function of the UV irradiation time t. All the $Abs^{\lambda max}(t)$ vs t plots have been adequately fitted using the biexponential rate law:

$$Abs^{\lambda max}(t) = -(A_1 + A_2) + A_1exp(-k^c_1t) + A_2exp(-k^c_2t) \quad (1)$$

with k^c_1 and k^c_2 the extracted coloration rate constants. In each case, k^c_1 describes the major contribution of the temporal evolution of the absorption, and it is quite pertinent to compare the photocoloration effects of the samples. Details of the kinetics parameters are given in Table SI4 in the Supporting Information. First, the photocoloration kinetics of the SN group has been compared for $\mathbf{MnMo_6O_{18}(SN)_2}$, $\mathbf{MnMo_6O_{18}(SP)(SN)}$ and **SNTris** (Fig. 8a). $\mathbf{MnMo_6O_{18}(SP)(SN)}$ and $\mathbf{MnMo_6O_{18}(SN)_2}$ have similar photocoloration rates (k^c_1 = 0.013 s^{-1} and k^c_2 = 0.002 s^{-1} for $\mathbf{MnMo_6O_{18}(SP)(SN)}$, k^c_1 = 0.011 s^{-1} and k^c_2 = 0.002 s^{-1} for $\mathbf{MnMo_6O_{18}(SN)_2}$). This could be tentatively explained considering that both materials show very similar structural arrangements, and the direct environments of the SN groups are comparable. It is also worth noting that, as expected from photographs, the photocoloration of $\mathbf{MnMo_6O_{18}(SP)(SN)}$ and $\mathbf{MnMo_6O_{18}(SN)_2}$ is faster and much more intense than that of **SNTris**. Hence, at first sight, the photoinduced ring-opening of the SN group should be much more effective in the two hybrid materials than in the pure organic one, the as-generated zwitterionic MC form being better stabilized in the polar hybrid frameworks. In addition, the $Abs^{570}(t)$ vs t plot of $\mathbf{MnMo_6O_{18}(SP)(SN)}$, characterizing the photocoloration of the SP moiety, has been compared with that of $\mathbf{MnMo_6O_{18}(SP)_2}$ (Fig. 8b).

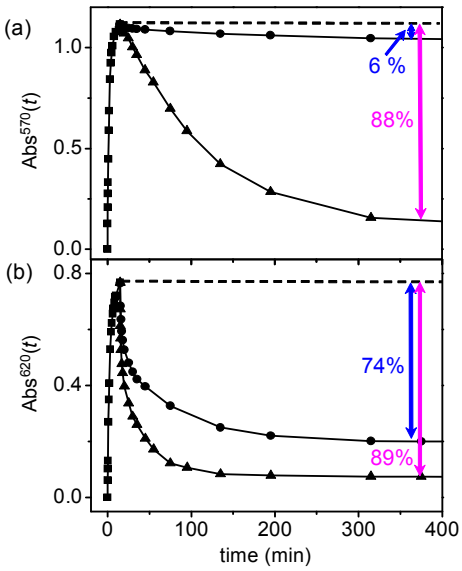

Fig. 9 Comparison of the temporal evolutions at room temperature of the absorbance (a) at λ_{max} = 570 nm for $\mathbf{MnMo_6O_{18}(SP)_2}$[10a], and (b) at λ_{max} = 620 nm for $\mathbf{MnMo_6O_{18}(SN)_2}$ under 365 nm-UV irradiation (■), in the dark during the thermal fading of a sample initially irradiated for 15 min under 365 nm-UV excitation (●), and under yellow light for a sample initially irradiated for 15 min under 365 nm-UV excitation (▲). The lines show the fits of the $Abs^{\lambda max}(t)$ *vs* t plots according to rate laws $Abs^{\lambda max}(t) = -(A_1 + A_2) + A_1exp(-k^c_1t) + A_2exp(-k^c_2t)$ for the photo-coloration process, and $Abs^{\lambda max}(t) = (A_0-A_1-A_2) + A_1exp(-k^f_1t) + A_2exp(-k^f_2t)$ for the two fading ones. The dashed line shows the absorbance value just before switching off the UV irradiation. The percents of absorbance lost after 6 hours in the dark (in blue) and under yellow light (in pink) are indicated.

The absorption at the end of the photocoloration process is less intense for $\mathbf{MnMo_6O_{18}(SP)(SN)}$, but the fast coloration rates of the SP groups are quite similar for both compounds (k^c_1 = 0.017 s^{-1} and k^c_2 = 0.004 s^{-1} for $\mathbf{MnMo_6O_{18}(SP)(SN)}$, k^c_1 = 0.015 s^{-1} and k^c_2 = 0.004 s^{-1} for $\mathbf{MnMo_6O_{18}(SP)_2}$). Focusing now on $\mathbf{(SP)_3MnMo_6O_{18}(SN)_2}$, the photocoloration kinetics of the SP^+ counter-cations in the hybrid material and in **(SP)I** have been compared (Fig. SI16 and Table SI4 in the Supporting Information), revealing that the photoinduced absorption of $\mathbf{(SP)_3MnMo_6O_{18}(SN)_2}$ reaches saturation much more faster than **(SP)I** (k^c_1 = 0.007 s^{-1} and 3.1 × 10^{-4} s^{-1} for $\mathbf{(SP)_3MnMo_6O_{18}(SN)_2}$ and **(SP)I**, respectively).

The color fading rates of $\mathbf{MnMo_6O_{18}(SN)_2}$, $\mathbf{MnMo_6O_{18}(SP)_2}$, $\mathbf{MnMo_6O_{18}(SP)(SN)}$ and $\mathbf{(SP)_3MnMo_6O_{18}(SN)_2}$ were

measured in the dark (thermal fading) and under yellow light, at room temperature, by monitoring the temporal decay of the photogenerated absorption bands of samples once irradiated under UV excitation for 15 minutes (i.e., a time for which the photoinduced absorption is quasi saturated). As already observed for other solid-state photochromic spiropyran/POM systems,[9c, 10b] decays can be well fitted using a biexponential rate law, with k^f_1 and k^f_2 the fading rate constants (k^f_1 describing the major contribution of the temporal evolution of the absorption) (see Tables SI5 and SI6 in the Supporting Information for detailed fading kinetic parameters).

Fig. 9 displays the $Abs^{570}(t)$ vs t and $Abs^{620}(t)$ vs t plots for **$MnMo_6O_{18}(SP)_2$** and **$MnMo_6O_{18}(SN)_2$**, respectively. Both materials develop strong different behaviours. The thermal bleaching process of **$MnMo_6O_{18}(SP)_2$** is very limited and undetectable with naked eyes. $Abs^{570}(t)$ decreases very slowly ($k^f_1 = 8.0 \times 10^{-5}$ s^{-1} and $k^f_2 = 0.006$ s^{-1}), and typically, the absorption loss is only 6% after 6 hours. This quite evidences that the main part of the zwitterionic MC form of the SP groups remains stabilized in the dark. In marked contrast, **$MnMo_6O_{18}(SN)_2$** develops a faster thermal fading process ($k^f_1 = 3.0 \times 10^{-4}$ s^{-1} and $k^f_2 = 0.010$ s^{-1}), and the absorption loss at $\lambda_{max} = 620$ nm is important (about 74% after 6 hours). For both materials, the bleaching at room temperature is considerably improved when the irradiated samples are exposed under yellow light i.e., with an energy near to that of the photogenerated absorption, (Table SI5 in the Supporting Information). The absorption loss is faster and reaches 88% after 6 hours for **$MnMo_6O_{18}(SP)_2$** (with $k^f_1 = 1.5 \times 10^{-4}$ s^{-1} and $k^f_2 = 1.5 \times 10^{-4}$ s^{-1}) and 89% for **$MnMo_6O_{18}(SN)_2$** ($k^f_1 = 7.0 \times 10^{-4}$ s^{-1} and $k^f_2 = 0.037$ s^{-1}). In addition, the material shows a good cyclability (Fig. SI17 in the Supporting Information). In the case of **$(SP)_3MnMo_6O_{18}(SN)_2$**, the thermal ring-closure process of the SP^+ counterions is slow ($k^f_1 = 4.0 \times 10^{-4}$ s^{-1} and $k^f_2 = 0.035$ s^{-1}), and typically, the absorption loss is limited to about 15% after 6 hours (Fig. SI18 in the Supporting Information), while under yellow light, the bleaching is strongly accelerated and the photoinduced absorption disappears from 200 min. This quasi-bistable system also shows a good cyclability (Fig. SI19 in the Supporting Information) and, to date, about 20 coloration/fading cycles at room temperature can be performed without detecting any fatigue resistance.

2.4 Temperature dependence solid-state photochromic properties

The thermal dependence of the solid-state photochromism of the hybrid materials has been investigated, starting with the symmetrical derivatives **$MnMo_6O_{18}(SN)_2$** and **$MnMo_6O_{18}(SP)_2$** in order to apprehend the influence of the grafted organic molecule.

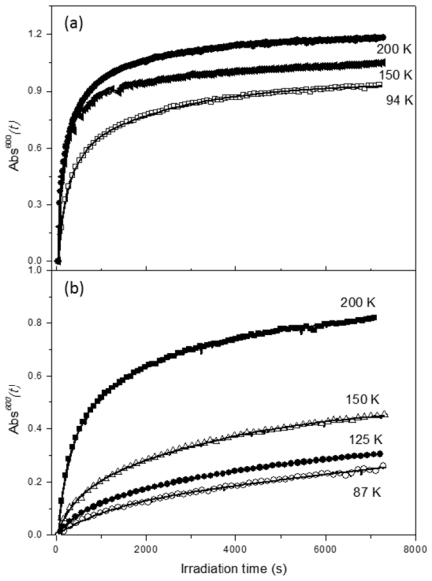

Fig. 10 (a) $Abs^{600}(t)$ vs. t plots for **$MnMo_6O_{18}(SP)_2$** at 200 K, 150 K and 94 K (b) $Abs^{600}(t)$ vs. t plots for **$MnMo_6O_{18}(SN)_2$** at 200 K, 150 K, 125 K and 87 K. The lines show the fits of the plots according to rate law $Abs^{600}(t) = -(A_1 + A_2) + A_1\exp(-k^c_1 t) + A_2\exp(-k^c_2 t)$.

Fig. 10 presents the evolution of the absorption at $\lambda = 600$ nm as a function of the UV irradiation time at different temperatures for **$MnMo_6O_{18}(SP)_2$** and **$MnMo_6O_{18}(SN)_2$**. We observed that the absorption signal can be fitted by the already described bi-exponential law (1) (see above) at several temperatures. The obtained parameter values for the coloration rate constants k^c_1, k^c_2 and the corresponding absorptions A_1 and A_2 are listed in Tables SI7 and SI8 in the Supporting Information. One can easily see the net difference of timescales between processes (1) and (2) characterized by k^c_1 and k^c_2 values respectively. Indeed, the process (1) takes place in the range of 10^3 s, while that of process (2) is almost ten times larger, which justify their decoupling. The coloration rate constants k^c_1 and k^c_2 increase with the temperature for both compounds. However, the photo-coloration of **$MnMo_6O_{18}(SN)_2$** is clearly more hindered at low temperature than that of **$MnMo_6O_{18}(SP)_2$**. The impact of temperature on **$MnMo_6O_{18}(SP)_2$** is weak and the sample may still be photo-excited significantly at 94K. Importantly, the global loss of efficiency in the photo-coloration phenomenon at low temperature for both hybrids compounds highly contrasts with previous results reported for pure organic spiro derivatives by Harada *et al.*.[18] So, the organization of the spiro entities in the structure (here, they are connected to an anionic inorganic platform that may better stabilize the polar merocyanine form) plays a crucial role for the thermal photochromic behavior.

The influence of the light intensity on the photo-coloration kinetics of **$MnMo_6O_{18}(SP)_2$** and **$MnMo_6O_{18}(SN)_2$** in isothermal conditions is reported in Supporting Information (Fig SI20 and SI21). In summary, the experiments show that the photo-transformation rate clearly increases with the

intensity of light, however the latter does not follow a linear behavior as expected for a single site process.

The thermal fading of $\mathbf{MnMo_6O_{18}(SP)_2}$ and $\mathbf{MnMo_6O_{18}(SN)_2}$ as function of the temperature have also been studied. First, the samples have been photo-excited at λ = 400 nm for one hour at 180 K. At this temperature, the thermal fading is negligible for both $\mathbf{MnMo_6O_{18}(SP)_2}$ and $\mathbf{MnMo_6O_{18}(SN)_2}$. Switching off the photoexcitation, the thermal evolution of the reflectance signal at λ = 600 nm was followed using a weak intensity beam to avoid any additional photo-induced relaxation. The temperature was raised with a thermal velocity of 0.3 K.min^{-1}. This procedure allowed estimating a temperature for which the thermal bleaching is effective.

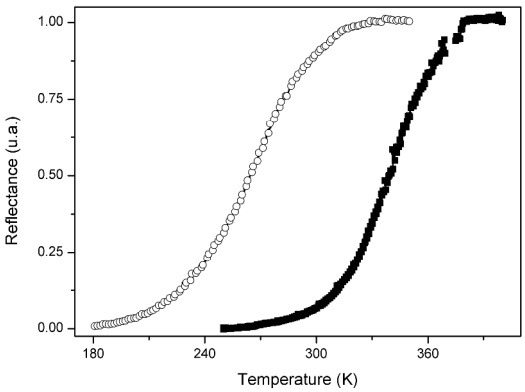

Fig. 11 Comparison of the thermal evolutions of the reflectance signal for $\mathbf{MnMo_6O_{18}(SN)_2}$ (o) and $\mathbf{MnMo_6O_{18}(SP)_2}$ (■). Temperature was changed with the rate 0.3 K.min^{-1} for both experiments.

Here again, the two materials present strong differences (as depicted in Fig. 11). In accordance with the previous results, the thermal fading process of $\mathbf{MnMo_6O_{18}(SP)_2}$ is quenched at room temperature and becomes effective above approximately 340 K. In contrast, the thermal fading of $\mathbf{MnMo_6O_{18}(SN)_2}$ is significant above 260 K, denoting a sizeable difference between the energy barrier values involved in the thermally-induced mechanism of both samples. For $\mathbf{MnMo_6O_{18}(SN)_2}$, the temporal evolution of the reflectance signal for different temperatures is precised in Fig. SI22 in the Supporting Information.

An inspection of the thermal curves of Fig. 11 shows that $\mathbf{MnMo_6O_{18}(SP)_2}$ has an equilibrium temperature located at ca. 340 K while that of $\mathbf{MnMo_6O_{18}(SN)_2}$ is found at ca. 260 K. The ratio, r, between these two values (r = 1.31) also represents the ratio between the corresponding energy barriers. This means that, possibly for steric reason, the thermal relaxation of $\mathbf{MnMo_6O_{18}(SP)_2}$ is slower than that of $\mathbf{MnMo_6O_{18}(SN)_2}$. Moreover, in a simple non-cooperative thermal relaxation process, the rate ln [(dAbs^{600}(T)/dT)/(Abs^{600}(T))] must be proportional to ($\Delta E/k_BT$) where ΔE is the macroscopic energy barrier. We have checked carefully this law and we found that both curves of Fig. 11 departure from the expected linear plot (not shown). This indicates clearly the existence of non-linear contributions whose origin can be attributed to (i) the presence of interactions (dipolar/electrostatic or steric/mechanical) between the photo-excited species or (ii) to the presence of light absorption inside the sample, leading to distribute spatially the relaxation times, thus resulting in nonlinear photo-excitation and thermal relaxation curves. Further investigations on thin films, for example, are necessary before to discriminate between those two mechanisms and to clarify the role of each of the quoted contributions.

3. Conclusion

The $\mathbf{MnMo_6O_{18}(SP)(SN)}$ compound reported herein thus represents a unique system associating in a single molecule three different switchable components. Using electrochemical techniques, it has been evidenced that in $\mathbf{MnMo_6O_{18}(SP)(SN)}$ the POM unit as well as the two different organic chromophores are redox active and that their redox processes can be discriminated, making $\mathbf{MnMo_6O_{18}(SP)(SN)}$ a remarkable electrochromic compound with multiple coloured states in solution. It has also been evidenced that this compound is a highly effective room temperature solid-state photochromic material, with a strong photocoloration contrast and a high coloration rate. The optical properties of the symmetrical $\mathbf{MnMo_6O_{18}(SP)_2}$ and $\mathbf{MnMo_6O_{18}(SN)_2}$ materials have also been studied. It has been found that all these systems exhibit very different photoresponses. Besides different coloration hues, it is worth noting that the thermal bleaching process of the $\mathbf{MnMo_6O_{18}(SP)_2}$ is very limited and undetectable with naked eyes, while $\mathbf{MnMo_6O_{18}(SN)_2}$ develops a fast thermal fading process, highlighting the complementarities of these last two compounds. Strikingly, it must be also underlined that while $\mathbf{MnMo_6O_{18}(SN)_2}$ develop a noticeable color-change effect in the solid state, the pure related organic reference **SNTris** is only very poorly photochromic, evidencing the crucial role of the POM on the optical properties of these materials. Importantly, it has been shown that $\mathbf{MnMo_6O_{18}(SN)_2}$ presents a good cyclability. This has also been demonstrated for the ionic compound $\mathbf{(SP)_3MnMo_6O_{18}(SN)_2}$ which possesses additional cationic spiropyran entities as counterions.

The thermal dependence of the photochromic behaviour of the reported materials has also been studied in a large temperature range. Even if such studies have been only very scarcely reported, we can emphasise that the global loss of efficiency in the photo-coloration phenomenon at low temperature found for these hybrids compounds highly contrasts with previous results reported for pure organic SP derivatives.[18] Moreover, the thermal behaviour of $\mathbf{MnMo_6O_{18}(SP)_2}$ and $\mathbf{MnMo_6O_{18}(SN)_2}$ differs noticeably, the fading process becoming significant above 260 K for $\mathbf{MnMo_6O_{18}(SN)_2}$ and 340 K for $\mathbf{MnMo_6O_{18}(SP)_2}$.

We are currently working to the elaboration of systems incorporating on the POM platform, in addition to photochromic molecules, other functional groups such as organic or inorganic fluorophores. The isolation of species incorporating organic chromophores initially stabilized in the merocyanine form will also be considered. Finally, the grafting

of this family of hybrid POMs on surface and on nanoparticles in order to elaborate sensors is also under study.

4. Experimental

General methods

All chemicals were used as purchased without purification: EEDQ (2-ethoxy-1-ethoxycarbonyl-1,2-dihydroquinoline), tris (2-amino-2-(hydroxyméthyl)propane-1,3-diol). The Mn-Anderson type polyoxomolybdates $(TBA)_3[MnMo_6O_{18}\{(OCH_2)_3CNH_2\}_2]$[16b], $(TBA)_3[MnMo_6O_{18}\{(OCH_2)_3CNHC_{21}H_{19}N_2O_4\}\{(OCH_2)_3CNH_2\}]$ (**$MnMo_6O_{18}$(SP)**)[10a] and the cationic spiropyran $(C_{20}H_{23}N_2O)I$ (**(SP)I**)[19] have been synthesized as previously described. The carboxylic acid SNCOOH[17] has been prepared following a slightly modified procedure. Elemental analyses were performed by the Service Central d'Analyse of CNRS, 69390 Vernaison, France. Infrared spectra (ATR) were recorded on an IRFT Nicolet 6700 apparatus. Relative intensities are given after the wavenumber as vs = very strong, s = strong, m = medium, w = weak, sh. = shoulder, br. = broad. NMR spectra were recorded on a Bruker Advance 300 spectrometer operating at 300 MHz for ^1H and 50 MHz for ^{13}C nuclei. Chemical shifts are expressed in parts per million (ppm) downfield from internal TMS. Nuclear magnetic resonance (NMR) spectra were recorded at 298 K. The following abbreviations were used to explain the multiplicities: s, singlet; d, doublet; t, triplet; br, broad peaks; m, multiplet or overlapping peaks.

The electrochemical set-up was an CHI660E driven by a PC with the CHI software. Potentials are measured against a saturated calomel reference electrode (SCE). The working electrode was a disk (3 mm diameter) of glassy carbon (GC). The counter electrode was a platinum gauze of large surface area. Ultra-pure DMF was purchased from Aldrich and used throughout. The solutions were deaerated thoroughly for at least 30 minutes with pure argon and kept under a positive pressure of this gas during the experiments. The supporting electrolyte was 0.2 M $LiClO_4$ in DMF. Spectroelectrochemical experiments were performed in a three-compartment cell comprising a 1-cm optical path quartz cuvette. The working electrode was a sheet of GC. The whole cell remained inserted in the spectrophometer cavity and kept under continuous argon bubbling and stirring during electrolyses. A second 1-cm quartz cell was matched with that of the electrochemical cell and served as a reference. UV-Visible spectra were recorded on a Shimazu U2550. Experiments were performed at the laboratory temperature. The bulk color sets shown in the main text were cut from the photos of the quartz cuvettes taken before or during the electrolyses.

Diffuse reflectance spectra were collected at room temperature on a finely ground sample with a Cary 5G spectrometer (Varian) equipped with a 60 mm diameter integrating sphere and computer control using the "Scan" software. Diffuse reflectance was measured from 250 to 1550 nm with a 2 nm step using Halon powder (from Varian) as reference (100% reflectance). The reflectance data were treated by a Kubelka-Munk transformation[20] to better locate the absorption thresholds. The samples were irradiated with a Fisher Bioblock labosi UV lamp (λ_{exc} = 365 nm, P = 6W). The photocoloration and fading kinetics were quantified by monitoring the temporal evolution of the absorption Abs(t) which was defined as Abs(t) = $-\log(R(t)/R(0))$, with R(t) and R(0) the reflectance at the time t and at t = 0, respectively.

Diffuse reflectance as function of temperature has been recorded with a home-made experimental set-up.[21] The latter is based on a multi-branch fiber optics assembly. The bundle is composed of detection fibers arranged in a circle around the illumination fibers. The light is detected on USB2000+ fiber optic spectrometer from Ocean Optics (200-850 nm, resolution ~1 nm). The bundle includes a reference leg which is used to monitor the illumination source, a 50W Xenon arc lamp. The sample is placed in a liquid nitrogen cryostat and the temperature was varied between 80 K and 400 K. The coloration and the fading of **$MnMo_6O_{18}(SP)_2$** and **$MnMo_6O_{18}(SN)_2$** have been investigated as function of the temperature and also for several intensities of illumination. We followed the various processes of photoexcitation and thermally-induced relaxation from the evolution of the reflectance spectra at λ = 600 nm which is close to the wavelength of maximum absorbance for the two compounds.

Synthesis

SNCOOH: 2,3,3-Trimethylindolenine (4.9 mL, 30.4 mmol) and 3-iodopropionic acid (6.084 g, 30.4 mmol) were heated at 100 °C for 3 h. The resulting solid material was dissolved in water, and the solution was washed with 45 mL of chloroform. Evaporation of water gave l-(β-carboxyethyl)-2,3,3-trimethylindolenine iodide (7.324 g, 20.4 mmol), which was used without further purification (67% yield).

The above iodide (6.000 g, 16.7 mmol), 1-nitrosonaphtol (2.890 g, 16.7 mmol) and triethylamine (2.36 mL, 16.7 mmol) were dissolved in 80 mL of ethanol. The resulting mixture was refluxed for 3 h. The solvent was removed under vacuum and the residue was dissolved in acetone. Charcoal was added to the solution and stirring was maintained during 1 h. After filtering, the solvent was removed under vacuum. Finally, the resulting solid was washed with acetonitrile and purified by crystallization in 100 mL of hot acetonitrile. **SNCOOH** was isolated as a yellow crystalline powder in 27% yield (1.750 g, 4.5 mmol).^1H NMR ($CDCl_3$, 300MHz, 298K) δ = 8.54 (d, $1H_{aro}$, J = 8.2 Hz), 7.79 (s, 1H, C*H*=N), 7.73 (d, $1H_{aro}$, J = 7.9 Hz), 7.66 (d, $1H_{aro}$, J = 8.9 Hz), 7.58 (m, $1H_{aro}$), 7.39 (m, $1H_{aro}$), 7.21 (m, $1H_{aro}$), 7.08 (m, $1H_{aro}$), 6.95 (m, $2H_{aro}$), 6.64 (br d, $1H_{aro}$, J = 9 Hz), 3.60 (m, 2H, N-CH_2), 2.66 (m, 2H, CH_2-COOH), 1.31 (s, 3H, CH_3), 1.29 (s, 3H, CH_3). IR (ATR) ν (cm^{-1}) 3282 (m), 2960 (ν C-H, m), 2944 (ν C-H, m), 2866 (ν C-H, m), 1699 (ν C=O, s), 1607 (m), 1591 (m), 1483 (s), 1456 (s), 1444 (s), 1351 (m), 1320 (m), 1285 (m), 1246 (s), 1167 (m),

1076 (m), 1038 (m), 999 (m), 887 (w), 813 (s), 753 (s), 741 (s), 684 (m), 590 (m), 574 (w), 520 (w).

SNTris: To a suspension of SNCOOH (0.535 g, 1.39 mmol) in EtOH (10 mL) were added EEDQ (0.415 g, 1.68 mmol) and tris (0.185 g, 1.53 mmol). The reaction mixture was stirred overnight at 60°C. On standing at room temperature for 2h, the product precipitated as a slightly blue powder. It was filtered and washed with ethanol and diethyl ether to give 0.395 g (0.81 mmol, 58% yield) of **SNTris**.
^{1}H NMR ($CDCl_3$, 300MHz, 298K) δ = 8.52 (d, 1H, J = 8.5 Hz), 7.79-7.75 (m, 2H), 7.71 (d, 1H, J = 9.0 Hz), 7.60 (m, 1H), 7.42 (m, 1H), 7.21 (m, 1H), 7.11 (d, 1H, J = 8.9 Hz), 7.08 (m, 1H), 6.91 (m, 1H), 6.72 (d, 1H, J = 7.9 Hz), 6.67 (br s, 1H, -N*H*-), 3.90-3.58 (br m, 5H, N-CH_2- and O*H*), 3.55 (br s, 6H, -CH_2OH), 2.72-2.58 (m, 1H, CH_2-C(O)), 2.50-2.37 (m, 1H, CH_2-C(O)), 1.33 (br s, 6H, -CH_3).
^{13}C NMR (DMSO, 50MHz, 298K) δ = 172.2 (-*C*(O)NH-), 153.1, 147.1, 144.1, 135.7, 130.6, 129.4, 128.4, 128.2, 127.7, 124.7, 122.7, 122.1, 121.6, 119.9, 117.3, 107.4, 99.6, 62.9, 60.9, 52.6, 35.8, 25.3, 20.8. IR (ATR) ν (cm^{-1}) 3284 (m), 2952 (ν C-H, m), 2925 (ν C-H, m), 2873 (ν C-H, m), 1632 (ν C=O, s), 1609 (m), 1592 (m), 1548 (s), 1482 (s), 1458 (m), 1382 (m), 1362 (m), 1305 (w), 1268 (m), 1246 (s), 1170 (m), 1115 (m), 1079 (s), 1042 (s), 1014 (s), 998 (s), 971 (m), 884 (w), 835 (w), 808 (s), 746 (s), 681 (s), 589 (m), 555 (w), 527 (w). Anal. calcd for $C_{28}H_{31}N_3O_5$ (%): C, 68.69; H, 6.38; N, 8.58. Found: C, 68.02; H, 6.41; N, 8.58.

(TBA)$_3$[MnMo$_6$O$_{18}${(OCH$_2$)$_3$CNHC$_{21}$H$_{19}$N$_2$O$_4$}{(OCH$_2$)$_3$CNHC$_{24}$H$_{21}$N$_2$O$_2$}] (MnMo$_6$O$_{18}$(SP)(SN)): To a solution of (TBA)$_3$[MnMo$_6$O$_{18}${(OCH$_2$)$_3$CNHC$_{21}$H$_{19}$N$_2$O$_4$}{(OCH$_2$)$_3$CNH$_2$}] (**MnMo$_6$O$_{18}$(SP)**) (0.42 g, 0.19 mmol) in CH_3CN (10 mL) were added SNCOOH (0.216 g, 0.56 mmol) and EEDQ (0.165 g, 0.67 mmol) at room temperature. The reaction mixture was stirred during one week. The solvent was removed under vacuum and the residue was dissolved in a minimum of CH_3CN. The solution was added to a large quantity of Et_2O (40 mL). The resulting precipitate was then isolated by filtration. This treatment was repeated four times (the last filtrate was no more coloured). Crystallization of the product by diffusion of diethyl ether into an acetonitrile solution gave suitable single crystals for X-ray diffraction. **MnMo$_6$O$_{18}$(SP)(SN)** (0.335 g, 0.13 mmol) was finally obtained in 67% yield. ^{1}H NMR (CD_3CN, 300MHz, 298K) δ = 8.56 (d, 1H, J = 8.2 Hz, H_{SN}), 8.06 (s, 1H, H_{SP}), 8.01 (d, 1H, J = 9.0 Hz, H_{SP}), 7.84-7.75 (m, 3H, H_{SN}), 7.60 (br t, 1H, J = 7.3 Hz, H_{SN}), 7.43 (br t, 1H, J = 7.5 Hz, H_{SN}), 7.22-7.11 (m, 5H, $2H_{SN}$ + $3H_{SP}$), 7.02 (d, 1H, J = 8.8 Hz, H_{SN}), 6.87 (m, 2H, $1H_{SN}$ + $1H_{SP}$), 6.72 (m, 3H, $1H_{SN}$ + $2H_{SP}$), 6.42 (br, 2H, -N*H*-), 5.88 (d, 1H, J =7.7 Hz, H_{SP}), 3.52 (br, 2H, N-CH_2-,$1H_{SN}$ + $1H_{SP}$), 3.33 (br, 2H, N-CH_2-,$1H_{SN}$ + $1H_{SP}$), 3.10 (m, 24H, CH_2 (TBA)), 2.85 (br, 1H, -CH_2-C(O), H_{SN}), 2.70 (br, 3H, -CH_2-C(O), $1H_{SN}$ + $2H_{SP}$), 1.61 (br, 24H, CH_2 (TBA)), 1.36 (m, 24H, CH_2 (TBA)), 1.29 (br s, 6H, -CH_3, H_{SN}), 1.24 (s, 3H, -CH_3, H_{SP}), 1.13 (s, 3H, -CH_3, H_{SP}), 0.97 (t, 36H, CH_3 (TBA)). *Note*: The protons of the spiropyran moiety are labeled H_{SP} while H_{SN} refers to the protons belonging to the spironaphthoxazine group. ^{13}C NMR (CD_3CN, 50MHz, 298K) δ 172.2 (-*C*(O)NH-, C_{SP}), 171.8 (-*C*(O)NH-, C_{SN}), 159.4 (C_{SP}), 152.6 (C_{SN}), 146.7 (C_{SN}), 143.8 (C_{SN}), 141.1 (C_{SP}), 136.1 (C_{SP}), 135.8 (C_{SN}), 130.8 (C_{SN}), 130.2 (C_{SN}), 129.3 (C_{SN}), 128.9 (C_{SP}), 128.0 (C_{SN}), 127.9 (C_{SN}), 127.8 (C_{SP}), 127.1 (C_{SN}), 125.6 (C_{SP}), 124.2 (C_{SN}), 123.5 (C_{SP}), 122.9 (C_{SP}), 122.8 (C_{SN}), 121.7 (C_{SN}), 121.6 (C_{SP}), 121.5 (C_{SN}), 119.7 (C_{SN}), 119.4 (C_{SP}), 119.1 (C_{SP}), 115.5 (C_{SP}), 107.7 (C_{SN}), 107.2 (C_{SP}), 107.1 (C_{SP}), 99.5 (C_{SN}), 58.4 (TBA), 52.6 (C_{SP}), 52.2 (C_{SN}), 41.1 (C_{SN}), 40.7 (C_{SP}), 33.8 (C_{SP}), 33.5 (C_{SN}), 26.1 (C_{SP}), 25.8 (C_{SN}), 23.4 (TBA), 20.0 (C_{SN}), 19.7 (TBA), 19.0 (C_{SP}), 13.2 (TBA). *Note*: The carbon atoms of the spiropyran moiety are labelled C_{SP} while C_{SN} refers to the carbon atoms belonging to the spironaphthoxazine group. Anal. calcd for $C_{101}H_{162}MnMo_6N_9O_{30}$ (%): C, 46.42; H, 6.24; N, 4.82; Mn, 2.10; Mo, 22.03. Found: C, 46.58; H, 6.23; N, 4.82; Mn, 1.95; Mo, 20.74.

(TBA)$_3$[MnMo$_6$O$_{18}${(OCH$_2$)$_3$CNHC$_{24}$H$_{21}$N$_2$O$_2$}$_2$] (MnMo$_6$O$_{18}$(SN)$_2$): To a solution of SNCOOH (1.476 g, 3.82 mmol) and EEDQ (1.030 g, 4.17 mmol) in CH_3CN (50 mL), (TBA)$_3$[MnMo$_6$O$_{18}${(OCH$_2$)$_3$CNH$_2$}$_2$] (1.800 g, 0.96 mmol) was added at room temperature. The reaction mixture was stirred during one week. The solvent was removed under vacuum and the residue was dissolved in a minimum of CH_3CN. The solution was added to a large quantity of Et_2O (80 mL). The resulting precipitate was then isolated by filtration. This treatment was repeated four times (the last filtrate was no more coloured). Crystallization of the product by diffusion of diethyl ether into an acetonitrile solution gave suitable single crystals for X-ray diffraction. **MnMo$_6$O$_{18}$(SN)$_2$** (2.15 g, 0.82 mmol) was finally obtained in 85% yield. ^{1}H NMR (CD_3CN, 300MHz, 298K) δ = 65.45 (br, 12H, CH_2-O-Mn), 8.57 (d, 2H, J = 8.2 Hz), 7.77 (m, 6H), 7.60 (t, 2H, J = 7.4 Hz), 7.43 (t, 2H, J = 7.8 Hz), 7.20 (m, 2H), 7.11 (m, 2H), 7.02 (m, 2H), 6.87 (t, 2H, J = 7.2 Hz), 6.75 (m, 2H), 6.38 (br, 2H, -C(O)N*H*-), 3.55 (br, 2H, CH_2-N), 3.35 (br, 2H, CH_2-N), 3.09 (m, 24H, CH_2 (TBA)), 2.84 (br, 2H, CH_2-C(O)), 2.74 (br, 2H, CH_2-C(O)), 1.59 (m, 24H, CH_2 (TBA)), 1.36 (m, 24H, CH_2 (TBA)), 1.29 (br s, 12H, CH_3), 0.97 (m, 36H, CH_3 (TBA)). ^{13}C NMR (CD_3CN, 50MHz, 298K) δ 171.7 (-*C*(O)NH-), 152.5, 146.7, 143.7, 135.7, 130.8, 130.2, 129.3, 128.0, 127.9, 127.2, 124.3, 122.7, 121.7, 121.5, 119.7, 107.6, 99.5, 58.3 (TBA), 52.2, 41.1, 33.5, 25.7, 23.5 (TBA), 20.0, 19.8 (TBA), 13.3 (TBA). IR (ATR) ν (cm^{-1}) 3298 (m), 2959 (ν C-H, m), 2932 (ν C-H, m), 2871 (ν C-H, m), 1676 (ν C=O, s), 1607 (w), 1508 (w), 1483 (s), 1457 (s), 1381 (m), 1362 (m), 1269 (m), 1112 (w), 1079 (m), 1019 (m), 938 (ν Mo=O, vs), 918 (ν Mo=O, vs), 900 (ν Mo=O, vs), 814 (s), 743 (s), 651 (ν Mo-O-Mo, br vs), 552 (s). Anal. calcd for $C_{104}H_{164}MnMo_6N_9O_{28}$ (%): C, 47.69; H, 6.31; N, 4.81; Mn, 2.10; Mo, 21.98. Found: C, 46.82; H, 6.36; N, 4.98; Mn, 2.05; Mo, 21.84.

(C$_{20}$H$_{23}$N$_2$O)$_3$[MnMo$_6$O$_{18}${(OCH$_2$)$_3$CNHC$_{24}$H$_{21}$N$_2$O$_2$}$_2$] (SP)$_3$MnMo$_6$O$_{18}$(SN)$_2$: To a solution of **(SP)I** (1.327 g, 3.06

mmol) in a co-solvent $CHCl_3$/ CH_3CN (1/3, v/v), a solution of **$MnMo_6O_{18}(SN)_2$** (0.400 g, 0.15 mmol) in CH_3CN (15 mL) was slowly added. After 1 h of stirring at room temperature, the solvent is removed under reduced pressure. The residue is partially dissolved in 5 mL of CH_3CN and the mixture is filtered. The filtrate is then added to a large quantity of Et_2O (60 mL). The precipitate is then dissolved in $CHCl_3$ (50 mL) and washed several times with water until the aqueous phase was uncoloured. After the organic phase was dried with $MgSO_4$, the solvent was removed. The residue was dissolved in a minimum of CH_3CN and the product was precipitated in a large amount of Et_2O. **$(SP)_3MnMo_6O_{18}(SN)_2$** (0.125 g, 0.04 mmol) was finally obtained in 29% yield. ^{1}H NMR (CD_3CN, 300MHz, 298K) δ = 64.91 (br, 12H, CH_2-O-Mn, H_{SN}), 8.50 (d, 2H, J = 7.9 Hz, H_{SN}), 7.75 (m, 6H, H_{SN}), 7.55-7.39 (br m, 13H, 4 H_{SN} + 9 H_{SP+}), 7.18-7.10 (br m, 10H, 4 H_{SN} + 6 H_{SP+}), 7.02 (d, 2H, J = 8.3 Hz, H_{SN}), 6.87 (m, 5H, 2 H_{SN} + 3 H_{SP+}), 6.74 (br, 2H, H_{SN}), 6.62-6.48 (br m, 8H, 6 H_{SN} + 2 H_{SP+}), 4.09 (s, 9H, H_{SP+}), 3.48 (br, 2H, N-CH_2, H_{SN}), 3.30 (br, 2H, N-CH_2, H_{SN}), 2.84 (br, 2H, -CH_2-C(O), H_{SN}), 2.74 (br s, 11H, 2 H_{SN} + 9 H_{SP+}), 2.63 (s, 9H, H_{SP+}), 1.29 (s, 12H, H_{SN}), 1.26 (s, 9H, H_{SP+}), 1.17 (s, 9H, H_{SP+}). *Note*: The protons of the cationic spiropyran are labeled H_{SP+} while H_{SN} refers to the protons belonging to the spironaphthoxazine moiety. ^{13}C NMR (CD_3CN, 50MHz, 298K) δ 171.9 (-C(O)NH-, C_{SN}), 152.9 (C_{SN}), 151.5 (C_{SP+}), 147.9 (C_{SP+}), 147.3 (C_{SP+}), 146.7 (C_{SN}), 143.8 (C_{SN}), 135.7 (C_{SN}), 135.6 (C_{SP+}), 134.6 (C_{SP+}), 131.6 (C_{SP+}), 130.7 (C_{SN}), 130.5 (C_{SP+}), 130.2 (C_{SN}), 129.3 (C_{SN}), 128.8 (C_{SP+}), 128.0 (C_{SN}), 127.9 (C_{SN}), 127.2 (C_{SN}), 124.2 (C_{SN}), 122.8 (C_{SN}), 122.2 (C_{SP+}), 121.6 (C_{SN}), 121.5 (C_{SN}), 120.1 (C_{SP+}), 119.7 (C_{SN}), 107.7 (C_{SN}), 107.2 (C_{SP+}), 106.2 (C_{SP+}), 99.5 (C_{SN}), 52.9 (C_{SP+}), 52.2 (C_{SN}), 41.5 (C_{SP+}), 41.1 (C_{SN}), 33.6 (C_{SN}), 29.1 (C_{SP+}), 25.9 (C_{SN}), 25.2 (C_{SP+}) , 21.1 (C_{SP+}), 20.1 (C_{SN}), 19.5 (C_{SP+}). *Note*: The carbon atoms of the cationic spiropyran are labelled C_{SP+} while C_{SN} refers to the carbon atoms belonging to the spironaphthoxazine moiety. IR (ATR) ν (cm^{-1}) 3283 (m), 2963 (ν C-H, m), 2927 (ν C-H, m), 2868 (ν C-H, m), 1672 (ν C=O, s), 1606 (s), 1552 (w), 1484 (s), 1457 (s), 1384 (m), 1363 (m), 1297 (s), 1269 (m), 1169 (w), 1109 (m), 1079 (m), 1059 (m), 1020 (s), 938 (ν Mo=O, vs), 918 (ν Mo=O, vs), 901 (ν Mo=O, vs), 814 (s), 743 (s), 656 (ν Mo-O-Mo, br vs), 551 (s). Anal. calcd for $C_{116}H_{125}MnMo_6N_{12}O_{31}.3H_2O$ (%): C, 48.58; H, 4.60; N, 5.86. Found: C, 48.42; H, 4.78; N, 5.72.

Acknowledgements

This work was supported by the CNRS, the Ministère de l'Enseignement Supérieur et de la Recherche, the ANR-11-BS07-011-01 BIOOPOM and the National Natural Science Foundation of China (No.21371173). Caroline Abreu is gratefully acknowledged for her participation to the synthesis of the SN derivatives.

Notes and references

[a] Institut Lavoisier de Versailles, UMR CNRS 8180, Université de Versailles Saint-Quentin, 45 avenue des Etats-Unis, 78035 Versailles Cedex (France). E-mail: olivier.oms@uvsq.fr.

[b] Institut des Matériaux Jean Rouxel, Université de Nantes, CNRS, 2 rue de la Houssinière, BP 32229, 44322 Nantes Cedex (France). E-mail: remi.dessapt@cnrs-imn.fr.

[c] Groupe d'Etude de la Matière Condensée, Bâtiment Fermat, Université de Versailles Saint-Quentin, 45 avenue des Etats-Unis, 78035 Versailles Cedex (France).

[d] Key Laboratory of Green Process Engineering, Institute of Process Engineering, Chinese Academy of Sciences, 100049 Beijing, (China). E-mail: zhanggj@home.ipe.ac.cn.

[e] Retired.

† Electronic Supplementary Information (ESI) available: ^{1}H and ^{13}C NMR spectra, cyclic voltammograms, Kubelka-Munk transformed reflectivity and absorption spectra, UV-vis absorption spectra in solution, additional photographs, photocoloration and fading kinetics parameters. CCDC 985599 and 985600. See DOI: 10.1039/b000000x/

1 a) Polyoxometalate Chemistry: From Topology via Self-Assembly to Applications (Eds M. T. Pope, A. Müller), KLUWER, Dordrecht, Netherlands, 2001; b) Polyoxometalate Chemistry for Nano-Composite Design, (Eds. T. Yamase, M. T. Pope), KLUWER, New York, 2002; c) Polyoxometalate Molecular Science, (Eds J. J. Borras-Almenar, E. Coronado, A. Müller, M. T. Pope), KLUWER, Dordrecht, Netherlands, NATO Science Series II, Vol. 98, 2003; d) D.-L. Long, R. Tsunashima and L. Cronin, *Angew. Chem. Int. Ed.*, 2010, **49**, 1736; e) U. Kortz, A. Müller, J. van Slageren, J. Schnack, N. S. Dalal and M. Dressel, *Coord. Chem. Rev.*, 2009, **253**, 2315.

2 a) Polyoxometalates in Catalysis, (Ed. C. L. Hill), *J. Mol. Catal. A*, 2007, **262**, 1; b) N. Mizuno and N. Misono, *Chem. Rev*., 1998, **98**, 199.

3 a) J. T. Rhule, C. L. Hill, D. A. Judd and R. F. Schinazi, *Chem. Rev*., 1998, **98**, 327; b) R. Prudent, V. Moucadel, B. Laudet, C. Barette, L. Lafanechere, B. Hasenknopf, J. Li, S. Bareyt, E. Lacote, S. Thorimbert, M. Malacria, P. Gouzerh and C. Cochet *Chem. Biol*., 2008, **15**, 683; c) H. El Moll, W. Zhu, E. Oldfield, L. M. Rodriguez-Albelo, P. Mialane, J. Marrot, N. Vila, I. M. Mbomekallé, E. Rivière, C. Duboc and A. Dolbecq, *Inorg. Chem*., 2012, **51**, 7921; d) F. Pu, E. Wang, H. Jiang and J. Ren, *Mol. Biosyst*., 2013, **9**, 113.

4 a) J. M. Clemente-Juan, E. Coronado and A. Gaita-Ariño, *Chem. Soc. Rev*., 2012, **41**, 7464; b) P. Kögerler, B. Tsukerblat and A. Müller, *Dalton Trans*., 2010, **39**, 21; c) O. Oms, A. Dolbecq and P. Mialane, *Chem. Soc. Rev.*, 2012, **41**, 7497.

5 Y.-F. Song and R. Tsunashima, *Chem. Soc. Rev*., 2012, **41**, 7384.

6 a) T. Yamase, *Chem. Rev*., 1998, **98**, 307; b) T. He and J. Yao, *Prog. Mater. Sci*., 2006, **51**, 810; c) R. Dessapt, M. Collet, V. Coué, M. Bujoli-Doeuff, S. Jobic, C. Lee and M.-H. Whangbo, *Inorg. Chem*., 2009, **48**, 574; d) A. Wutkowski, B. R. Srinivasan, A. R. Naik, C. Schütt, C. Näther and W. Bensch, *Eur. J. Inorg. Chem*., 2011, 2254; e) H. El Moll, A. Dolbecq, I. Martyr Mbomekallé, J. Marrot, P. Deniard, R. Dessapt and P. Mialane, *Inorg. Chem*., 2012, **51**, 2291.

7 K. Hakouk, O. Oms, A. Dolbecq, H. El Moll, J. Marrot, M. Evain, F. Molton, C. Duboc, P. Deniard, S. Jobic, P. Mialane and R. Dessapt, *Inorg. Chem*., 2013, **52**, 555.

8 a) G. Berkovic, V. Krongrauz and V. Weiss, *Chem. Rev*., 2000, **100**, 1741; b) V. I. Minkin, *Chem. Rev*., 2004, **104**, 2751.

9 a) P. Mialane, G. J. Zhang, I. M. Mbomekallé, P. Yu, J. -D. Compain, A. Dolbecq, J. Marrot, F. Sécheresse, B. Keita and L. Nadjo, *Chem. Eur. J*., 2010, **16**, 5572; b) J.-D. Compain, P. Deniard, R. Dessapt, A. Dolbecq, O. Oms, F. Sécheresse, J. Marrot and P. Mialane, *Chem. Commun*., 2010, **46**, 7733 ; c) K. Hakouk, O. Oms, A. Dolbecq, J. Marrot, A. Saad, P. Mialane, H. El Bekkachi, S. Jobic, P. Deniard, and R. Dessapt, *J. Mater. Chem. C* 2014, **2**, 1628.

10 a) O. Oms, K. Hakouk, R. Dessapt, P. Deniard, S. Jobic, A. Dolbecq, T. Palacin, L. Nadjo, B. Keita, J. Marrot and P. Mialane, *Chem. Commun*., 2012, **48**, 12103; b) A. Parrot, G. Izzet, L.-M. Chamoreau, A. Proust, O. Oms, A. Dolbecq, K. Hakouk, H. El Bekkachi, P. Deniard, R. Dessapt and P. Mialane, *Inorg. Chem*., 2013, **52**, 11156.

11 a) S. Kawauchi, H. Yoshida, N. Yamashina, M. Ohira, S. Saeda and M. Irie, *Bull. Chem. Soc. Jpn*., 1990, **63**, 267; b) N. Y. C. Chu, *Sol. Energy Mater*., 1986, **14**, 215.

12 W. Yuan, L. Sun, H. Tang, Y. Wen, G. Jiang, W. Huang, L. Jiang, Y. Song, H. Tian and D. Zhu, *Adv. Mater*., 2005, **17**, 156.

13 a) Z. Zhang, C. Zhang, M. Fan and W. Yan, *Dyes Pigm*., 2008, **77**, 469; b) H. Song, K. Chen and H. Tian, *Dyes Pigm*., 2005, **67**, 1.

14 M. M. Paquette, R. A. Kopelman, E. Beitler and N. L. Frank, *Chem. Commun*., 2009, 5424.

15 a) A. Dolbecq, E. Dumas, C. R. Mayer and P. Mialane, *Chem. Rev*., 2010, **110**, 6009; b) A. Proust, B. Matt, R. Villaneau, G. Guillemot, P. Gouzerh, G. Izzet, *Chem. Soc. Rev*., 2012, **41**, 7605

16 a) B. Hasenknopf, R. Delmont, P. Herson and P. Gouzerh, *Eur. J. Inorg. Chem*., 2002, **5**, 1081; b) P. R. Marcoux, B. Hasenknopf, J. Vaissermann and P. Gouzerh, *Eur. J. Inorg. Chem*., 2003, **13**, 2406; c) C. Allain, S. Favette, L.–M. Chamoreau, J. Vaissermann, L. Ruhlmann and B. Hasenknopf, *Eur. J. Inorg. Chem*., 2008, **22**, 3433; d) Y.–F. Song, D.–L. Long, S. E. Kelly, L. Cronin, *Inorg. Chem*., 2008, **47**, 9137; e) Y. –F. Song, N. McMillan, D. –L. Long, S. Kane, J. Malm, M. O. Riehle, C. P. Pradeep, N. Gadegaard and L. Cronin, *J. Am. Chem. Soc*., 2009, **131**, 1340; f) Y. Yan, H. Wang, B. Li, G. Hou, Z. Yin, L. Wu and V. W. W. Yam, *Angew. Chem. Int. Ed*., 2010, **49**, 9233; g) M. H. Rosnes, C. Musumeci, C. P. Pradeep, J. S. Mathieson, D.–L. Long, Y.–F. Song, B. Pignataro, R. Cogdell and L. Cronin, *J. Am. Chem. Soc*., 2010, **132**, 15490; h) M.–P. Santoni, A. K. Pal, G. S. Hanan, A. Proust and B. Hasenknopf, *Inorg. Chem*., 2011, **50**, 6737; i) B. Liu, J. Yang, M. Yang, Y. Wang, N. Xia, Z. Zhang, P. Zheng, W. Wang, I. Lieberwirth and C. Kübel, *Soft Matter*, 2011, **7**, 2317; j) P. Wu, P. Yin, J. Zhang, J. Hao, Z. Xiao and Y. Xei, *Chem. Eur. J*., 2011, **17**, 12002; k) J. Thiel, D. Yang, M. H. Rosnes, X. Liu, C. Yvon, S. E. Kelly, Y. –F. Song, D. –L. Long and L. Cronin, *Angew. Chem. Int. Ed*., 2011, **50**, 8871; l) Z. He, Y. Yan, B. Li, H. Ai, H. Wang, H. Li and L. Wu, *Dalton Trans*., 2012, **41**, 10043; m) C. Allain, D. Schaming, N. Karakostas, M. Erard, J.-P. Gisselbrecht, S. Sorgues, I. Lampre, L. Ruhlmann and B. Hasenknopf, *Dalton Trans*., 2013, **42**, 2745; n) C. Yvon, A. Macdonell, S. Buchwald, A. J. Surman, N. Follet, J. Alex, D.-L. Long and L. Cronin, *Chem. Sci.*, 2013, **4**, 3810.

17 X. Li, Y. Wang, T. Matsuura and J. Meng, *Heterocycles*, 1999, **51**, 2639.

18 J. Harada, Y. Kawazoe and K. Ogawa, *Chem. Commun*., 2010, **46**, 2593.

19 S. Bénard and P. Yu, *Adv. Mater.*, 2000, **12**, 48.

20 P. Kubelka and F. Munk, *Z. Techn. Physik*, 1931, **12**, 593.

21 W. Morscheidt, J. Jeftic, E. Codjovi, J. Linares, A. Bousseksou, H. Constant-Machado and F. Varret, *Meas. Sci. Technol.*, 1998, **9**, 1311.

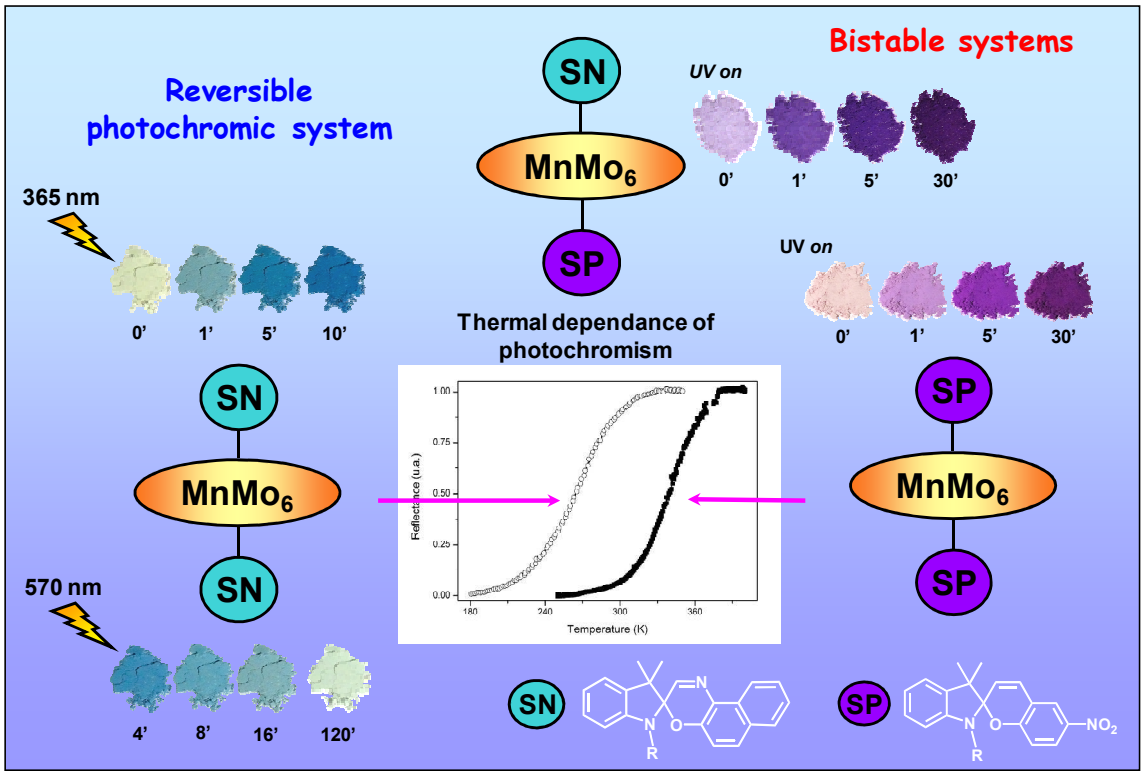

Optical studies in a large temperature range of triads incorporating polyoxometalate, spiropyran and spironaphtoxazine components highlight the richness and complementarities of the photochromic properties of these hybrid materials.